10

SCATTERING FROM AN ARBITRARY CYLINDER IN THE PRESENCE OF A PARALLEL PLANAR MEDIA INTERFACE USING THE BYMOMENT METHOD

R. Lee and A. C. Cangellaris

10.1 Introduction

The bymoment method, which is a method to handle the truncation of the mesh for boundary value problems in unbounded regions using the finite-element method, has previously been applied to arbitrary cylinders in free space [1,2]. In this paper we will show that the method can be extended to a case where the cylinder is not in free space. The specific geometry that we choose is a cylinder in the presence of two semi-infinite half-spaces. This geometry is chosen because of its application to such areas as geophysics, radar design, microwave or high speed integrated circuits, and target identification. Because of

the versatility of the finite-element method in handling geometries with *arbitrary shapes* and *inhomogeneities*, it is a powerful tool for studying the problem of electromagnetic scattering from arbitrary cylinders. Unfortunately, there is very little available in the literature on the application of the finite-element method to the interface problem because of the difficulty in accounting for the interface when the mesh is truncated. To date, the only published work involving the finite-element method that also accounts for the interface is the one done by Chang and Mei [3]. This work is specialized to a body of revolution and is not applicable to the infinitely long cylinder.

Most of the past work on the interface problem involved other techniques. Some of the earliest investigations were done by Hohmann [4] and Parry and Ward [5]. They applied integral equation methods to obtain numerical solutions to homogeneous cylinders. Howard [6] and Mahmoud, Ali, and Wait [7] used a multipole expansion of the scattered field to obtain a solution. Howard and Kretzschmar [8] developed a technique which they called the volume current method. Recently, a method of moments approach was adopted by Butler, Xu and Glisson [9]. This work was further extended by Xu and Butler [10,11].

In the following discussion, we begin with a description of the geometry. Next, we formulate the general theory for the bymoment method. An expression for the testing functions is introduced. These testing functions satisfy the correct boundary conditions along the interface and at infinity. A discussion is given on the choice of the locations of the testing functions. Finally, we compare our finite-element solution, using the bymoment method for the truncation of the mesh, to method of moments results in the literature. The purpose of these results are to validate the bymoment method rather than to show the capabilities of the method. In fact, the method of moments is more efficient for perfectly conducting cylinders, whereas the finite-element method is more efficient for penetrable bodies. Because we could not find many results involving penetrable bodies near a media interface, most of the comparisons are for perfectly conducting cylinders. Several results for penetrable cylinders are given to show the versatility of the finite-element method.

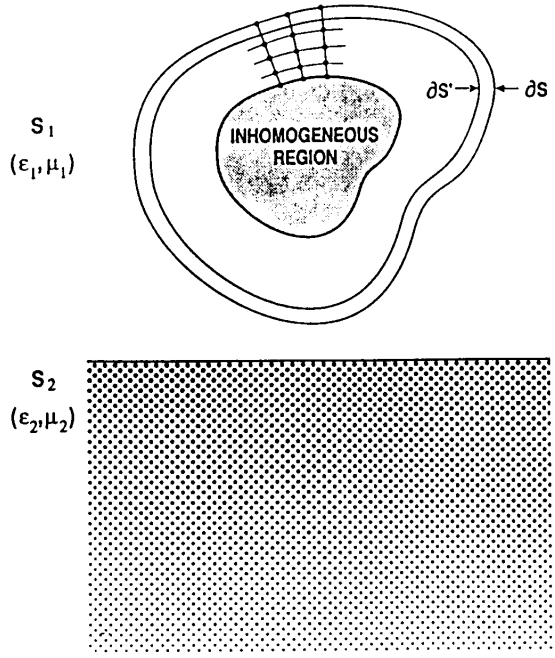

Figure 10.1 Geometry of an arbitrary cylinder in the presence of an interface.

10.2 Theory

Let us consider the case of an infinitely long cylinder in the presence of a media interface which divides the region into two half-spaces (Fig. 10.1). Although this figure shows the cylinder to be above the interface, we will also consider the case where the cylinder is wholly contained or partially buried in the lower half-space. The material properties of the upper half-space, exclusive of the cylinder, are that of free space. The material properties of the lower half-space are homogeneous and in general, may be either lossy or a pure dielectric. The permeability of the lower half-space is assumed to be that of free space ($\mu_2 = \mu_1 = \mu_0$). The coordinate system that we use is cartesian. Note that the coordinate system is oriented such that the z-axis is parallel to the axis of the cylinder. Since we are applying the finite-element method only over the region occupied by the cylinder, we define a mesh which totally encloses the cylinder. The mesh is constructed such that the elements on the boundary of the mesh are exterior to the cylinder. The boundary of the mesh is given by ∂S. The line $\partial S'$ follows a closed path which passes through the interior of all the elements on

the boundary of the mesh. Therefore $\partial S'$ is exterior to the cylinder. The significance of this line will be discussed later in this paper. We denote the region inside of ∂S by S_c, The upper half-space, exclusive of S_c, is defined to be S_1, and the remaining lower half-space is called S_2.

The material properties of the cylinder do not vary with z but are allowed to vary in a piece-wise constant fashion over the cylinder's cross-section. Let us choose a source which produces an incident field which is invariant in z. The resulting geometry is a two dimensional one. Therefore, the fields may be decoupled into a TM_z (E_z, H_x, H_y) polarization and a TE_z (H_z, E_x, E_y) polarization. The subscript indicates the fact that the transverse direction is with respect to z. This leads to the following Helmholtz equation:

$$\left(\nabla^2 + k_i^2\right)\begin{pmatrix} E_z \\ H_z \end{pmatrix} = 0 \tag{1}$$

where we choose E_z for the TM_z case and H_z for the TE_z case. The operator ∇^2 is the Laplacian in x and y. The wave number is given by $k_i = k_0\sqrt{\mu_{ri}\epsilon_{ri}}$ with the subscript i denoting the region where the Helmholtz equation is evaluated, i.e., k_c for S_c, k_1 for S_1, and k_2 for S_2. Note that (1) holds inside each element of the finite element grid used in the discretization of S_c, which agrees with our original assumption of piece-wise element-by-element material property variation. In general, we assume that the relative dielectric constant incorporates the conduction loss and is given by $\epsilon_{ri} = \epsilon'_{ri} - i\sigma_i/\omega\epsilon_0$. The variable k_0 is the wave number in free space, and the $e^{i\omega t}$ time variation has been suppressed. Note that since S_1 is free space, $\epsilon_{r1} = 1$ and $\mu_{r1} = 1$.

Since the formulation for the TM_z and TE_z polarizations are virtually identical, only the TE_z case will be considered. On occasions where the two cases differ, we will show the steps for both.

a. Boundary Conditions on ∂S

To determine the set of boundary conditions on ∂S, we must first develop the notation for representing a function on the mesh boundary. Let us introduce a variable t which varies from 0 to d where d is the length of ∂S. We may then represent H_z along ∂S by a function of the single variable t with each value of t corresponding to a point on ∂S. Let us call this function $h_s(t)$. Note that since the points $t = 0$ and $t = d$ correspond to the same point on ∂S, $h_s(0) = h_s(d)$. We

may write $h_s(t)$ in terms of a complete set of linearly independent functions $\Psi_n(t)$ as follows:

$$h_s(t) = \sum_{n=1}^{\infty} a_n \Psi_n(t), \qquad t \in [0, d] \tag{2}$$

where a_n are unknown coefficients. Since we must numerically solve our problem, the summation in (2) must be truncated to a finite number of terms which we define to be N. The value of N depends upon the convergence requirements and the choice of basis functions Ψ_n.

b. Finite-Element Solution

Let us consider the finite element problem in S_c where the solution on ∂S is known. Since the solution on ∂S is known, H_z in S_c can be found by using a standard finite-element formulation of an interior Dirichlet boundary value problem. We use the method of weighted residuals [12] to formulate the finite-element expression. This guarantees that the Helmholtz equation in (1) is true in the weak sense. We can write the expression as follows:

$$\iint \left[(\nabla^2 + k_c^2) H_z \psi_j\right] dS = 0 \tag{3}$$

where the weighting functions ψ_j $(j = 1,2,...)$ constitute a set of first order differentiable, real scalar functions which we choose. By using Green's first identity, expression (3) becomes

$$\iint \left[\nabla H_z \cdot \nabla \psi_j - k_c^2 H_z \psi_j\right] dS - \int \left(\psi_j \hat{n} \cdot \nabla H_z\right) d\ell = 0 \tag{4}$$

where $\hat{n}$ is the outward unit normal. To obtain the solution for H_z, we evaluate (4) over each element in the mesh. By applying the boundary conditions on the fields at the interfaces between adjacent elements, we can nullify the contributions from the line integral along these inter-element boundaries. Noting that since both H_z and $\hat{n} \cdot \nabla H_z / \epsilon_{rc}$ are continuous between elements, we obtain the following equation from (4):

$$\iint \frac{1}{\epsilon_{rc}} \left[\nabla H_z \cdot \nabla \psi_j - k_c^2 H_z \psi_j\right] dS = 0 \tag{5}$$

Similarly, for the TM_z case, we obtain

$$\iint \frac{1}{\mu_{rc}} \left[\nabla E_z \cdot \nabla \psi_j - k_c^2 E_z \psi_j\right] dS = 0 \tag{6}$$

where we have applied the continuity of both E_z and $\hat{n} \cdot \nabla E_z/\mu_{rc}$. Note that the line integral along ∂S does not vanish. However, since we are solving the Dirichlet problem, the weighting functions ψ_j are chosen to be zero on ∂S; hence, the line integral along ∂S is zero and does not enter into the formulation.

Let us now consider the situation where the solution on ∂S is not known, as is actually the case. From the uniqueness theorem we know that, with the presence of any physical loss mechanism, the fields inside a given volume are determined uniquely by either the tangential electric or tangential magnetic fields on the surface enclosing the volume [13]. Therefore, the field in S_c is uniquely determined by h_s. From (2) we see that we can represent h_s by N basis functions, each of which is multiplied by an unknown coefficient a_n. If we solve N finite-element problems with $\Psi_n(t)$ $(n = 1, 2, \ldots, N)$ as the boundary condition for the nth finite-element problem, we obtain N numerical finite-element solutions which form a basis for the magnetic field in S_c. We shall call each of the finite-element solutions a *finite-element basis function.* We denote the finite-element basis functions by $\Lambda_n(x, y)$ for $(x, y) \in S_c$. Because of linearity and the uniqueness theorem, we can write the H_z as a superposition of the finite-element basis functions multiplied by the appropriate coefficient a_n. The expression is given by

$$H_z(x, y) = \sum_{n=1}^{N} a_n \Lambda_n(x, y), \quad (x, y) \in S_c \tag{7}$$

The coefficients a_n are determined by coupling the interior solution to the properties of the exterior region.

c. *Determination of Coefficients*

To evaluate the coefficients, we must first define additional surfaces in our geometry. Let the surface enclosed by $\partial S'$ be denoted by S_c'. We also define S_e' to be the surface exterior to $\partial S'$.

The field in S_e' can be divided into the incident field and the scattered field. This is written as

$$H_z(x, y) = H_z^{inc}(x, y) + H_z^{sc}(x, y), \quad (x, y) \in S_e' \tag{8}$$

where the scattered field satisfies the Helmholtz equation,

$$\left(\nabla^2 + k_i^2\right) H_z^{sc}(x,y) = 0, \quad (x,y) \in S_e' \tag{9}$$

and the Sommerfeld radiation condition at infinity. The incident field H_z^{inc} is defined to be the field everywhere in the absence of the cylinder. This definition of the incident field implies that the boundary conditions for the continuity of the tangential electric and magnetic field at the interface are satisfied by H_z^{sc}.

Let Φ_j $(j = 1,2,\ldots,N)$ be a set of N linearly independent testing functions which are chosen to satisfy the Helmholtz equation over the surface S_e', i.e.,

$$\left(\nabla^2 + k_i^2\right) \Phi_j(x,y) = 0, \quad (x,y) \in S_e' \tag{10}$$

and the radiation condition at infinity. Applying Green's theorem for H_z^{sc} and Φ_j/ϵ_{ri} over the region denoted by the intersection of S_e' and the upper half-space and the region denoted by the intersection of S_e' and the lower half-space, we obtain the following expression by using (9) and (10):

$$\begin{aligned}
&\int_{\partial S'} \frac{1}{\epsilon_{ri}} \left[\Phi_j \frac{\partial H_z^{sc}}{\partial n} - H_z^{sc} \frac{\partial \Phi_j}{\partial n} \right] d\ell + \\
&\int_{\partial S_{int}} \frac{1}{\epsilon_{r1}} \left[\Phi_j^{(+)} \frac{\partial H_z^{sc(+)}}{\partial n} - H_z^{sc(+)} \frac{\partial \Phi_j^{(+)}}{\partial n} \right] d\ell - \\
&\int_{\partial S_{int}} \frac{1}{\epsilon_{r2}} \left[\Phi_j^{(-)} \frac{\partial H_z^{sc(-)}}{\partial n} - H_z^{sc(-)} \frac{\partial \Phi_j^{(-)}}{\partial n} \right] d\ell = 0
\end{aligned} \tag{11}$$

where ∂S_{int} denotes the plane interface and the superscripts $(+)$ and $(-)$ denote the values of the field quantities just above and just below the interface, respectively. Note that the contributions of the line integral at infinity vanishes in (11) since both H_z^{sc} and Φ_j satisfy Sommerfeld's radiation condition. Since H_z^{sc} satisfies the interface boundary conditions which are given by

$$H_z^{sc(+)} = H_z^{sc(-)} \tag{12a}$$

$$\frac{1}{\epsilon_{r1}} \frac{\partial H_z^{sc(+)}}{\partial n} = \frac{1}{\epsilon_{r2}} \frac{\partial H_z^{sc(-)}}{\partial n} \tag{12b}$$

we observe that the contribution from the line integral along the interface will vanish if we choose Φ_j such that they satisfy (12a) and (12b) also. This leaves only the line integral term,

$$\int_{\partial S'} \frac{1}{\epsilon_{ri}} \left[\Phi_j \frac{\partial H_z^{sc}}{\partial n} - H_z^{sc} \frac{\partial \Phi_j}{\partial n} \right] d\ell = 0 \tag{13}$$

By substituting (8) into (13) and then using (7), we may write the following equation:

$$\sum_{n=1}^{N} a_n \int_{\partial S'} \frac{1}{\epsilon_{ri}} \left[\Phi_j \frac{\partial \Lambda_n}{\partial n} - \Lambda_n \frac{\partial \Phi_j}{\partial n} \right] d\ell = \int_{\partial S'} \frac{1}{\epsilon_{ri}} \left[\Phi_j \frac{\partial H_z^{inc}}{\partial n} - H_z^{inc} \frac{\partial \Phi_j}{\partial n} \right] d\ell \tag{14}$$

The expressions for both H_z^{inc} and Φ_j are known. We can therefore obtain expressions for $\partial H_z^{inc}/\partial n$ and $\partial \Phi_j/\partial n$. Also, the numerical values for both Λ_n and $\partial \Lambda_n/\partial n$ along $\partial S'$ can be obtained from the finite-element solution. We chose the line integral in (14) to be along $\partial S'$ rather than ∂S since it was found that more accurate results were obtained when the integral was evaluated along the interior of the elements.

The only unknowns left in (14) are the coefficients a_n. By using the N testing functions Φ_j, we can form an $N \times N$ matrix equation to solve for the coefficients. We write the matrix equation as follows:

$$\begin{pmatrix} S_{11} & S_{12} & \cdots & S_{1N} \\ S_{21} & S_{22} & \cdots & S_{2N} \\ \vdots & \vdots & \ddots & \vdots \\ S_{N1} & S_{N2} & \cdots & S_{NN} \end{pmatrix} \begin{pmatrix} a_1 \\ a_2 \\ \vdots \\ a_N \end{pmatrix} = \begin{pmatrix} T_1 \\ T_2 \\ \vdots \\ T_N \end{pmatrix} \tag{15}$$

where S_{jn} and T_j are given by

$$S_{jn} = \int_{\partial S'} \frac{1}{\epsilon_{ri}} \left[\Phi_j \frac{\partial \Lambda_n}{\partial n} - \Lambda_n \right] d\ell \tag{16}$$

$$T_j = \int_{\partial S'} \frac{1}{\epsilon_{ri}} \left[\Phi_j \frac{\partial H_z^{inc}}{\partial n} - H_z^{inc} \frac{\partial \Phi_j}{\partial n} \right] d\ell \tag{17}$$

10.3 Calculation of Testing Functions

Up to now we have not specified the testing functions Φ_j. For a cylinder in free space, Cangellaris and Lee [1] gave two possible sets of solutions for Φ_j. One set of solutions was the cylindrical harmonic functions. The other was a set of free space Green's functions with the sources located in S_c'. For the half-space problem, we will choose the latter method to obtain our solution. The Green's function for the half-space problem is well known for an electric line source (TM_z case) and is given by Felsen and Marcuvitz [14]. Similarly, the solution for a magnetic line source (TE_z case) can be easily obtained. In order to differentiate between the two solutions, let g^J be the Green's function due to an electric line source, and let g^M be the Green's function due to a magnetic line source. The geometry for the Green's function problem is the same as that in Fig. 10.1 except with the cylinder absent. Therefore, S_1 encompasses the entire upper half-space, and S_2 encompasses the entire lower half-space.

a. TM_z Case

Let us consider the problem of an electric line source of unity strength located in S_1. We must therefore solve the following differential equation:

$$-\left(\nabla^2 + k_i^2\right) g_{i1}^J\Big(x, y|x', y'\Big) = \delta\Big(x - x'\Big)\delta\Big(y - y'\Big), \qquad i = 1, 2 \quad (18)$$

where the primed coordinates indicate the location of the source and the unprimed coordinates indicate the observer location. The subscript $i1$ of the Green's function indicates that the observation point is in S_i and the source location is in S_1. Since we are considering an electric line source, g_{i1}^J must satisfy the boundary conditions of E_z and $\partial E_z/\partial n$ along the interface. The resulting solution for the observation point in S_1 is given by

$$g_{11}^J\left(x, y|x', y'\right) = \frac{1}{4i} H_0^{(2)}\left(k_1|\bar{r} - \bar{r}'|\right) + \frac{1}{\pi}\int_0^\infty \frac{u_1 - u_2}{2u_1\left(u_1 + u_2\right)} e^{-u_1(y+y')} \cos k_x\left(x - x'\right) dk_x \qquad (19)$$

where $|\bar{r} - \bar{r}'| = \sqrt{(x - x')^2 + (y - y')^2}$ and $u_i = \sqrt{k_x^2 - k_i^2}$; Re $(u_i) > 0$. The form of (19) is not the same as that given by Felsen and Marcuvitz because the above form is more suitable for numerical evaluation [15]. Also, we have corrected for differences in coordinate system and time variation definitions. In studying the expression in (19), we note that the first term represents the Green's function in the absence of the interface, and the second term represents the reflection from the interface. The solution in S_2 is given by

$$g_{21}^J\left(x, y|x', y'\right) = \frac{1}{\pi}\int_0^\infty \frac{e^{-u_1 y'} e^{u_2 y}}{u_1 + u_2} \cos k_x(x - x')\, dk_x \qquad (20)$$

To obtain the Green's functions for the line source in S_2, we simply have to switch u_1 and u_2 and replace (y, y', k_1) by $(-y, -y', k_2)$. Then (19) becomes the solution for the observation point in S_2, and (20) becomes the solution for the observation point in S_1.

To determine the values of the Green's functions we must numerically evaluate the integrals in (19) and (20). This is done by repeated application of Gauss quadrature integration on finite subintervals along the real axis until a specific convergence is achieved. Because of the highly oscillatory behavior and slow decay of the integrand as a function of k_x, the evaluation of the integral is both tedious and computationally expensive. For most problems, the majority of the computational time is spent evaluating the testing functions rather than the finite-element solutions. Thus, it is very important to minimize the testing function calculations. Several techniques are utilized to improve the convergence of the integral [16], including asymptotic extraction and variable transformations.

b. TE_z Case

For a magnetic line source of unit strength in S_1, we have the following differential equation:

$$-\left(\nabla^2 + k_i^2\right) g_{i1}^M\left(x, y|x', y'\right) = \delta\left(x - x'\right)\delta\left(y - y'\right), \qquad i = 1, 2 \quad (21)$$

The definitions are the same as that in the TM_z case except that g_{i1}^M must satisfy the boundary conditions for H_z and $\partial H_z/\partial n$ at the interface. The resulting solution for the observation point in S_1 is given by

$$g_{11}^{M}\left(x,y|x'y'\right) = \frac{1}{4i}H_0^{(2)}\left(k_1|\bar{r}-\bar{r}'|\right)+$$
$$\frac{1}{\pi}\int_0^{\infty}\frac{\epsilon_r u_1 - u_2}{2\epsilon_r u_1(u_1+u_2)}e^{-u_1(y+y')}\cos k_x(x-x')dk_x \qquad (22)$$

where we define $\epsilon_r = \epsilon_{r2}/\epsilon_{r1}$. Since $\epsilon_{r1} = 1$, we see that $\epsilon_r = \epsilon_{r2}$. The solution for the observation point in S_2 is given by

$$g_{21}^{M}\left(x,y|x',y'\right) = \frac{1}{\pi}\int_0^{\infty}\frac{\epsilon_r e^{-u_1 y'}e^{u_2 y}}{\epsilon_r u_1 + u_2}\cos k_x(x-x')\,dk_x \qquad (23)$$

For a line source in S_2, we make the same modifications as in the TM_z case. In addition, we replace ϵ_r by $1/\epsilon_r$. To numerically evaluate the TE_z Green's functions, we use the same numerical techniques as those used to evaluate the TM_z Green's functions.

We may now relate the Green's functions to the testing functions Φ_j. Since the Green's function must satisfy the Helmholtz equation in S_e', we locate the line source in S_c'. Let $\{x_j, y_j\}$, $j = 1,2,\ldots,N$ be points in S_c'. Then for the TE_z case

$$\Phi_j = g_{im}^{M}\left(x,y|x_j,y_j\right), \qquad i,m = 1,2 \qquad (24)$$

where the subscript im indicates whether the observation and source locations are above or below the interface. This results in N linearly independent testing functions for any choice of $(x_j, y_j) \in S_c'$ as long as the locations of the line sources are different for each j. Unfortunately, the locations of the sources cannot be chosen arbitrarily. This is analogous to the situation in the method of moments. Consider the case where we apply collocation to a method of moments problem. Then the basis functions are pulse functions given by

$$P_n(x) = \begin{cases} 1, & x_{n-1} < x < x_n \\ 0, & \text{otherwise} \end{cases} \qquad (25)$$

where x_{n-1} and x_n denote the boundary of the nth $(n = 1,\ldots,N)$ pulse. The weighting functions are delta functions located at $x = y_i$, $i = 1,\ldots,N$. The location of the delta functions cannot be arbitrary. In fact, for the case where $y_i \notin (x_{n-1}, x_n)$ for all values of i,

the resulting matrix is ill-conditioned. Thus, we must place y_i such that $y_i \in (x_{n-1}, x_n)$ for $i = n$. From this example, we see that although ideally the location of the line sources can be chosen anywhere in S_c', realistically some care must be taken in choosing their location. The choice for the placement of the testing functions is not quite as obvious as in the method of moments example. In the numerical results section, a procedure is described for choosing the location of the line sources.

By substituting our Green's function expressions into (14), we obtain

$$\sum_{n=1}^{N} a_n \int_{\partial S'} \frac{1}{\epsilon_{ri}} \left[g_{im}^M \frac{\partial \Lambda_n}{\partial n} - \Lambda_n \frac{\partial g_{im}^M}{\partial n} \right] d\ell = \int_{\partial S'} \frac{1}{\epsilon_{ri}} \left[g_{im}^M \frac{\partial H_z^{inc}}{\partial n} - H_z^{inc} \frac{\partial g_{im}^M}{\partial n} \right] d\ell \tag{26}$$

The normal derivative of the Green's function $\partial g_{im}^M / \partial n$ is determined by evaluating the Green's function at the nodes of the elements which contain $\partial S'$ and then numerically calculating the derivative along $\partial S'$. Because we choose the Green's function to be the testing function, the right-hand side of (26) can be simplified since

$$\frac{1}{\epsilon_{ri}} H_z^{inc} = - \int_{\partial S'} \frac{1}{\epsilon_{ri}} \left[g_{im}^M \frac{\partial H_z^{inc}}{\partial n} - H_z^{inc} \frac{\partial g_{im}^M}{\partial n} \right] d\ell \tag{27}$$

c. Far-Field Expressions (TM_z Case)

Once we determine the solution of E_z in S_c, we can obtain an expression for the E_z^{sc} in S_1 and S_2 from Green's theorem. This is given by

$$E_z^{sc}(x,y) = \int_{\partial S'} \left[g_{im}^J \Big(x, y | x', y' \Big) \frac{\partial E_z(x', y')}{\partial n'} - E_z \Big(x', y' \Big) \frac{\partial g_{im}^J (x, y | x', y')}{\partial n'} \right] d\ell' \tag{28}$$

In general, the above form is rather complicated since the Green's function must be evaluated numerically. We can simplify (28) by considering a far-field approximation for the Green's function. In order

to do this, let us modify the Green's function expression in (19) and rewrite it into the form,

$$g_{11}^{J}\left(x,y|x',y'\right) = \frac{1}{4\pi}\int_{-\infty}^{\infty}\frac{1}{u_1}\left[e^{-u_1|y-y'|}+R(k_x)e^{-u_1(y+y')}\right]e^{-ik_x(x-x')}\,dk_x \tag{29}$$

where $R(k_x)=(u_1-u_2)/(u_1+u_2)$. Also from (20), we obtain

$$g_{21}^{J}\left(x,y|x',y'\right) = \frac{1}{4\pi}\int_{-\infty}^{\infty}\frac{1}{u_1}\left[1+R(k_x)\right]e^{-u_1y'+u_2y}e^{-ik_x(x-x')}\,dk_x \tag{30}$$

We can similarly modify the Green's function due to a line source in S_2. We now apply the *method of steepest descent* [14] to our Green's functions. This results in the following far-field expressions:

$$g_{11}^{J}\sim\sqrt{\frac{1}{8\pi}}\,e^{i\pi/4}\,e^{ik_1x'\sin\phi}\left[e^{ik_1y'\cos\phi}+R_1e^{-ik_1y'\cos\phi}\right]\frac{e^{-ik_1\rho}}{\sqrt{k_1\rho}} \tag{31a}$$

$$g_{21}^{J}\sim\sqrt{\frac{1}{8\pi}}\,e^{i\pi/4}\left[1+R_2\right]e^{-ik_2x'\sin\tilde{\phi}}\,e^{-ik_1y'\sqrt{1-\epsilon_{r2}\sin^2\tilde{\phi}}}\,\frac{e^{-ik_2\rho}}{\sqrt{k_2\rho}} \tag{31b}$$

$$g_{12}^{J}\sim\sqrt{\frac{1}{8\pi}}\,e^{i\pi/4}\left[1+R_1\right]e^{ik_1x'\sin\phi}\,e^{-ik_2y'\sqrt{1-\sin^2\tilde{\phi}/\epsilon_{r2}}}\,\frac{e^{-ik_1\rho}}{\sqrt{k_1\rho}} \tag{31c}$$

$$g_{22}^{J}\sim\sqrt{\frac{1}{8\pi}}\,e^{i\pi/4}\,e^{-ik_2x'sin\tilde{\phi}}\left[e^{-ik_2y'cos\tilde{\phi}}+R_2\,e^{ik_2y'cos\tilde{\phi}}\right]\frac{e^{-ik_2\rho}}{\sqrt{k_2\rho}} \tag{31d}$$

where we have used the definitions $x=\rho\sin\phi, y=\rho\cos\phi$ and $\tilde{\phi}=\phi-\pi$. Thus, the angle $\phi=0$ represents the positive y-axis. The reflection terms are defined by

$$R_1=\frac{cos\phi-\sqrt{\epsilon_{r2}-sin^2\phi}}{cos\phi+\sqrt{\epsilon_{r2}-\sin^2\phi}} \tag{32a}$$

$$R_2=\frac{cos\tilde{\phi}-\sqrt{1/\epsilon_{r2}-sin^2\tilde{\phi}}}{cos\tilde{\phi}+\sqrt{1/\epsilon_{r2}-sin^2\tilde{\phi}}} \tag{32b}$$

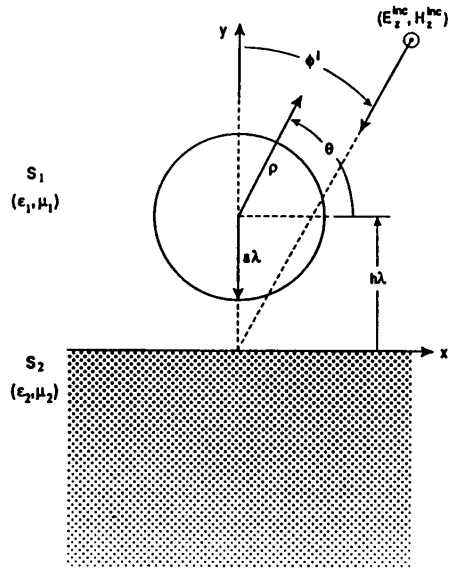

Figure 10.2 Geometry of a circular cylinder in the presence of an interface.

In performing the steepest descent integral, we ignored the contributions due to the branch cut. If we choose ρ sufficiently large, the branch cut contribution is only significant at the grazing angles which are at $\phi = \pi/2$ or $\phi = -\pi/2$. Therefore, by substituting (31*a*) through (31*d*) into (28), we can obtain an accurate far-field expression for E_z^{sc} as long as ϕ is not too close to grazing.

10.4 Numerical Results

Although our method allows us to solve the problem with a cylinder of any arbitrary cross-section and material properties, most of the results are only for simple geometries so that our results can be compared to those available in the literature. The numerical computations were performed on a VAX 2000 workstation. The mesh generator was written by T.D. Blacker [17]. First order quadrilateral isoparametric elements are used for all the finite-element computations in this paper. The bymoment method allows us to choose a mesh which only extends one element outside the cylinder. We find that this is true even for cylinders with sharp corners.

The numerical results are given in terms of a normalized surface current j^{norm} for the perfectly conducting circular cylinder and a normalized far-field expression for the dielectric circular cylinder. The surface currents are normalized to the incident magnetic field at a specific point on the cylinder. For the TE_z case, the normalized surface current is given by

$$j_\theta^{norm}(\theta) = \frac{H_z(\lambda a, \theta)}{H_z^{inc}(\lambda a, \theta_a)} \tag{33}$$

where the ρ, θ cylindrical coordinate system is centered on the cylinder with the angle θ defined in the usual manner as shown in Fig. 10.2. The radius of the cylinder is specified to be $\rho/\lambda = a$ where λ is the free space wavelength. The cylinder is centered at the point $x/\lambda = 0$, $y/\lambda = h$. For cylinders which are totally or partially in the upper half-space, we define $\theta_a = 90°$. For cylinder which are totally in the lower half-space, we define $\theta_a = -90°$. For the TM_z case, where the incident magnetic field is given by $H_t^{inc}\hat{t}$, we obtain the following expression for the normalized surface current:

$$j_z^{norm}(\theta) = \frac{H_\theta(\lambda a, \theta)}{H_t^{inc}(\lambda a, \theta_a)} \tag{34}$$

H_θ and H_t^{inc} can be obtained from the derivatives of E_z and E_z^{inc}, respectively. Note that since the derivatives of E_z must be obtained by numerical evaluation inside the finite element mesh, we calculate H_θ at the centroid of the elements bordering the cylinder rather than on the element boundary at the surface of the cylinder. Therefore, the results for the TM_z case have some inaccuracies. To minimize these inaccuracies, we keep the elements which border the cylinder small. For the TE_z case, this inaccuracy does not exist since H_z is calculated on the nodes along the cylinder. For the dielectric cylinder (TM_z), the normalized far-field expression is

$$\left|E_z^{ff}(\theta)\right| = \lim_{\rho \to \infty} \frac{|E_z^{sc}(\rho, \theta)|}{|E_{max}(\rho, \theta)|} \tag{35}$$

where $|E_{max}(\rho, \theta)|$ is defined to be the maximum value of $|E_z^{sc}(\rho, \theta)|$ as $\rho \to \infty$ for all values of θ. We substitute the far-field expression from (31*a*) through (31*d*) into (28) to determine E_z^{sc}. We observe that $0 \leq |E_z^{ff}| \leq 1$.

We define the incident field to be the field due to a uniform plane wave in the absence of the cylinder. Let us assume that the plane wave is travelling from the upper half-space into the lower half-space. The solution to this problem is well known [18]. For the TM_z case, we write

$$E_z^{inc} = \begin{cases} \left[e^{ik_1 y\cos\phi^i} + \Gamma_\perp e^{-ik_1 y\cos\phi^i}\right] e^{ik_1 x\sin\phi^i}, & y > 0 \\ \left[1+\Gamma_\perp\right] e^{ik_1(x\sin\phi^i + y\cos\phi^t)}, & y < 0 \end{cases} \tag{36}$$

where $\Gamma_\perp = (\cos\phi^i - \cos\phi^t)/(\cos\phi^i + \cos\phi^t)$ and $\cos\phi^t = \sqrt{\epsilon_r - \sin^2\phi^i}$. The angle ϕ^i is defined from the y-axis (Fig. 10.2). For the TE_z case,

$$H_z^{inc} = \begin{cases} \left[e^{ik_1 y\cos\phi^i} + \Gamma_{||} e^{-ik_1 y\cos\phi^t}\right] e^{ik_1 x\sin\phi^i}, & y > 0 \\ \left[1+\Gamma_{||}\right] e^{ik_1(x\sin\phi^i + y\cos\phi^t)}, & y < 0 \end{cases} \tag{37}$$

where $\Gamma_{||} = (\epsilon_r\cos\phi^i - \cos\phi^t)/(\epsilon_r\cos\phi^i + \cos\phi^t)$.

For all the results which follow, we use sinusoidal functions for the basis functions Ψ_n. The number of basis functions used varies from 12 to 24, depending on the electrical size of the cylinder. The source locations of the weighting functions are arranged inside the cylinder such that their pattern conforms to the boundary of the cylinder. For the case of a circular cylinder with radius a, we distribute the sources in a circular pattern with the radius of this circular pattern being $0.75a$. Results for a perfectly conducting circular cylinder were obtained by Butler, Xu, and Glisson [9] and Xu and Butler [10,11] for both the TM_z and TE_z cases using the method of moments. We will compare our results to theirs. In the numerical results which follow, the method of moment solutions are shown by the solid and dashed lines while the bymoment results are denoted by the triangular and asterisk symbols for the perfectly conducting cylinder cases. For the first dielectric cylinder case, the method of moment result is given by the solid line, and the bymoment result is given by the dashed line.

We begin by considering a perfectly conducting cylinder with $a = 0.175$. The lower half-space is a pure dielectric with $\epsilon_{r2} = 4$. A plane wave is assumed to be normally incident on the interface $(\phi^i = 0)$. Results were obtained from the method of moments [9,10] for $h = -0.175$ and $h = 0.175$. Because the cylinder contacts the interface only at one point, we could not obtain a suitable mesh for this geometry

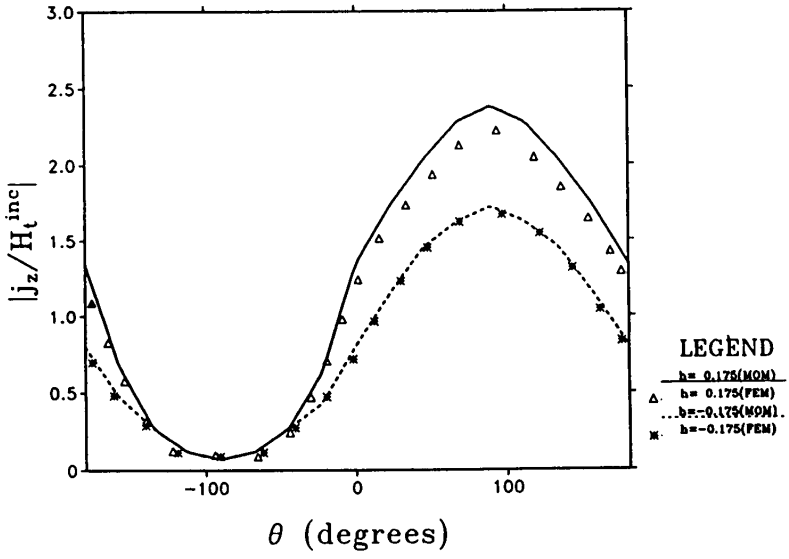

Figure 10.3 Magnitude of the normalized surface current density as a function of θ for $h = -0.175$ and $h = 0.175$. Parameters are $a = 0.175, \phi^i = 0, \epsilon_r = 4$ (TM_z case).

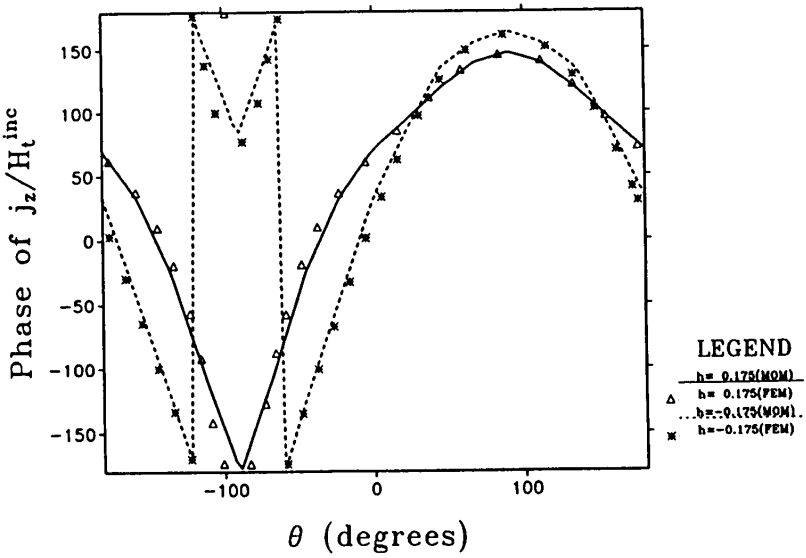

Figure 10.4 Phase of the normalized surface current density as a function of θ for $h = -0.175$ and $h = 0.175$. Parameters are $a = 0.175, \phi^i = 0, \epsilon_r = 4$ (TM_z case).

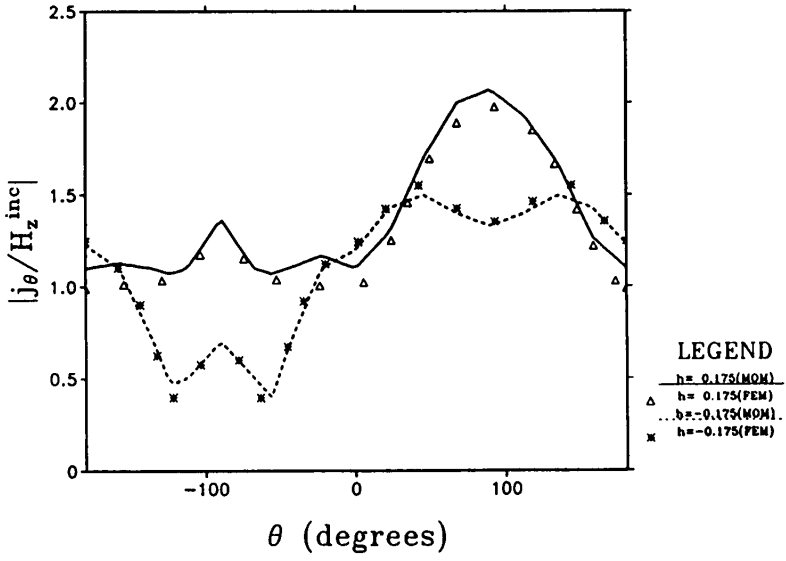

Figure 10.5 Magnitude of the normalized surface current density as a function of θ for $h = -0.175$ and $h = 0.175$. Parameters are $a = 0.175, \phi^i = 0, \epsilon_r = 4$ (TE_z case).

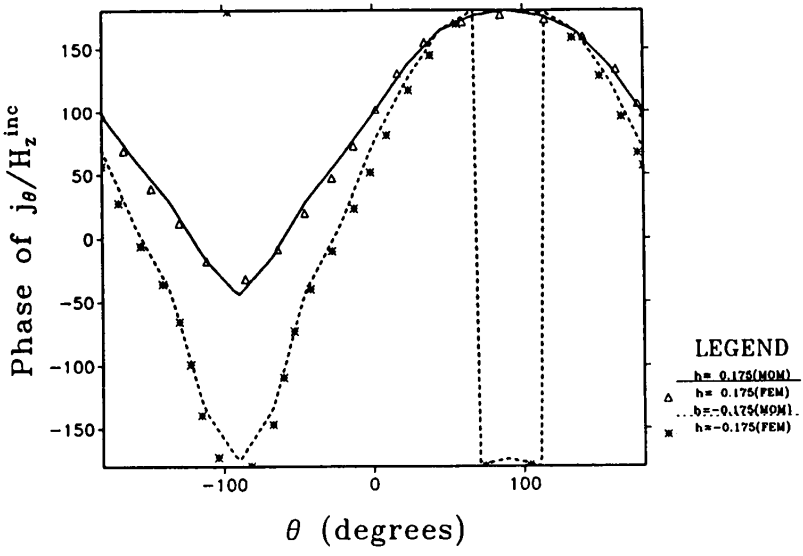

Figure 10.6 Phase of the normalized surface current density as a function of θ for $h = -0.175$ and $h = 0.175$. Parameters are $a = 0.175, \phi^i = 0, \epsilon_r = 4$ (TM_z case).

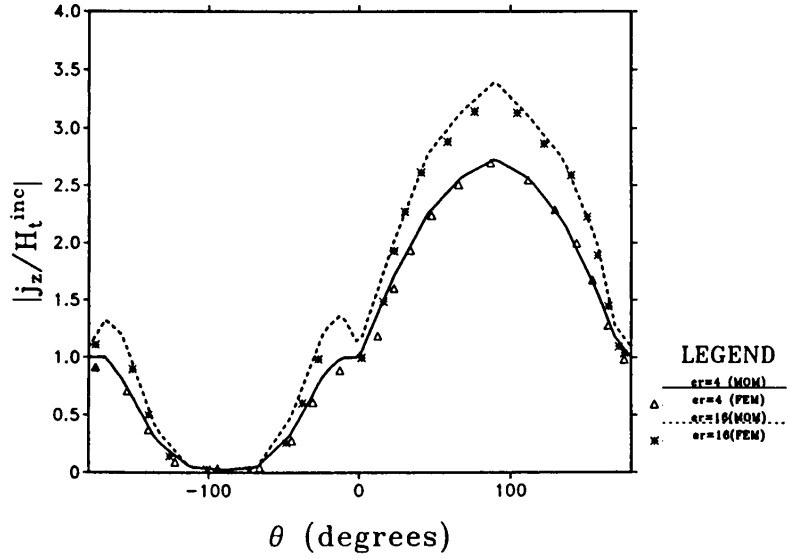

Figure 10.7 Magnitude of the normalized surface current density as a function of θ for $\epsilon = 4$ and $\epsilon_r = 16$. Parameters are $a = 0.375, \phi^i = 0, h = 0.425$ (TM_z case).

using quadrilateral elements. Therefore, we obtain a solution for $h = -0.185$ and $h = 0.185$ and assume that this small perturbation does not result in too drastic a change in the numerical results. This problem can be overcome by using triangular elements, but unfortunately, our mesh generator can only use quadrilaterals elements. For the TM_z case, a comparison between the two methods of the magnitude and phase of j_z as a function of θ are shown in Figs. 10.3 and 10.4. We observe that the agreement is very good for both the magnitude and phase. For the TE_z case, the magnitude and phase of j_θ are given in Figs. 10.5 and 10.6. Again, we see that there is good agreement between the method of moments and bymoment results. In addition, the agreement between the results indicate that the slight shift in the value of h did not adversely affect the results.

Let us now consider a geometry where we vary the material properties of the lower half-space rather than the cylinder position. For the parameters $h = 0.425$, $a = 0.375$, and $\phi^i = 0°$, we consider cases where $\epsilon_{r2} = 4$ and $\epsilon_{r2} = 16$. Figures 10.7 and 10.8 show the magnitude and phase of j_z for the TM_z case, and Figs. 10.9 and 10.10 give the magnitude and phase of j_θ for the TE_z case. The agreement between the two methods is excellent except for the phase plot of the

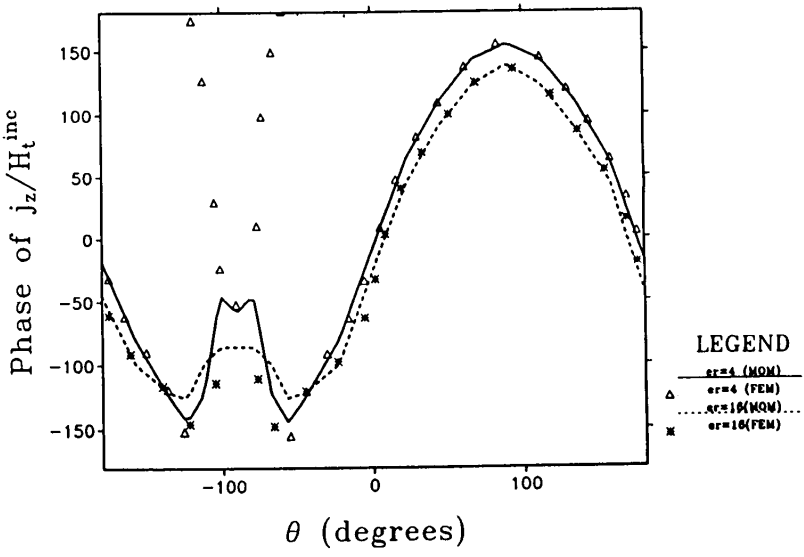

Figure 10.8 Phase of the normalized surface current density as a function of θ for $\epsilon_r = 4$ and $\epsilon_r = 16$. Parameters are $a = 0.375, \phi^i = 0, h = 0.425$ (TM_z case).

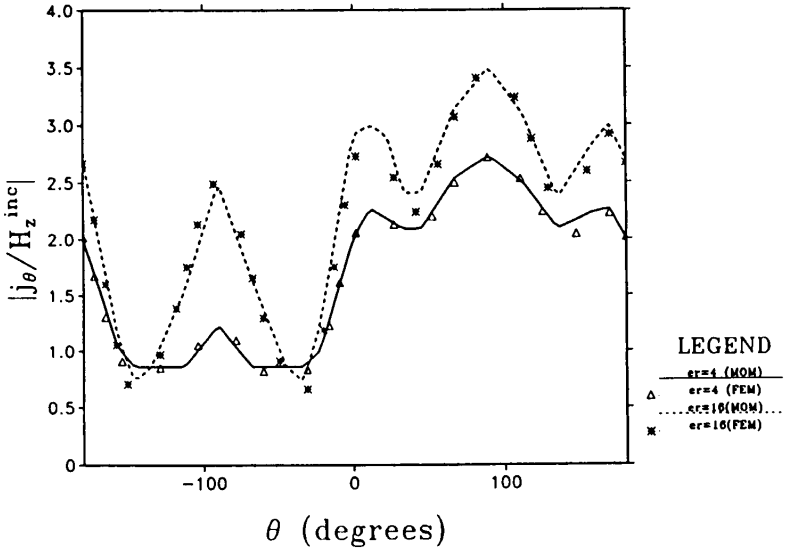

Figure 10.9 Magnitude of the normalized surface current density as a function of θ for $\epsilon_r = 4$ and $\epsilon_r = 16$. Parameters are $a = 0.375, \phi^i = 0, h = 0.425$ (TE_z case).

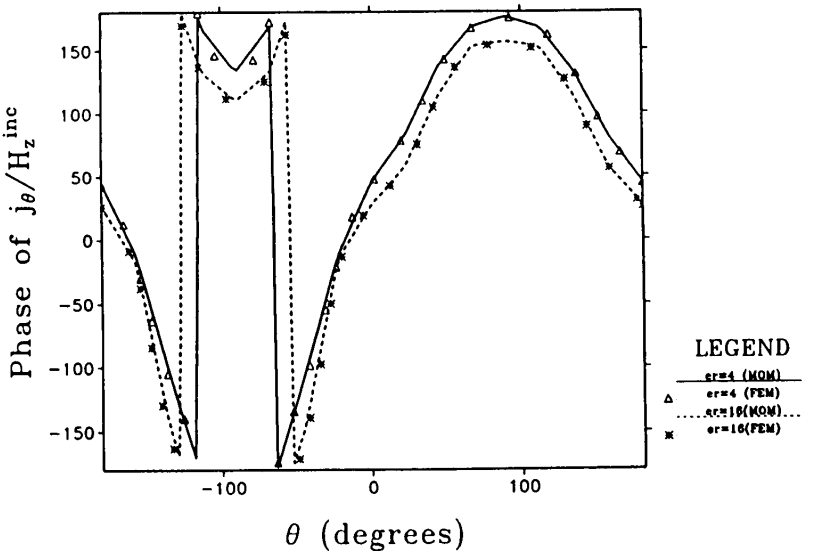

Figure 10.10 Phase of the normalized surface current density as a function of θ for $\epsilon_r = 4$ and $\epsilon_r = 16$. Parameters are $a = 0.375, \phi^i = 0, h = 0.425$ (TE_z case).

TM_z case with $\epsilon_r = 4$. In the region near $\theta = -90°$, there is a discrepancy between the two solutions. Note that in this region, the magnitude of the j_z/H_t^{inc} is very close to zero. Therefore, we believe the phase error is due to numerical computation errors rather than errors in the method.

To show the variation with angle of incidence, solutions are obtained for $\phi^i = 0°$ and $\phi^i = 60°$. For these solutions we only have method of moment results for the TM_z case [11]. Therefore, let us only consider this polarization. The perfectly conducting circular cylinder under consideration has a radius given by $a = 0.125$. We specify $\epsilon_{r2} = 4$ and $h = -0.065$. Figures 10.11 and 10.12 give the results for both the magnitude and phase of j_z.

For the case of the homogeneous dielectric cylinder with TM_z polarization, we have method of moments results [19] for $|E_z^{ff}(\theta)|$ where $a = 0.175$, $h = -0.175$, $\epsilon_r = 4$, and $\phi^i = 0°$. The cylinder has a relative dielectric constant given by $\epsilon_{rd} = 8$. Again, because the cylinder is only touching the interface at one point, we solve the problem using the bymoment method with $h = -0.185$. A comparison of the two methods is shown in Figure 10.13. The next case involves a larger dielectric cylinder ($a = 0.6$, $h = -0.65$, $\epsilon_r = 4$, $\epsilon_{rd} = 8$, and $\phi^i = 0°$).

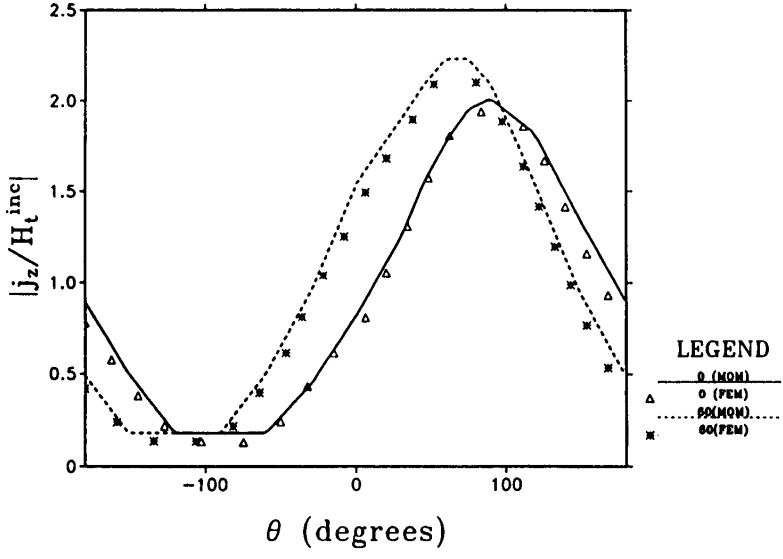

Figure 10.11 Magnitude of the normalized surface current density as a function of θ for $\phi = 0°$ and and $\phi^i = 60°$. Parameters are $a = 0.125$, $\epsilon_r = 4$, $h = -0.065$ (TM_z case).

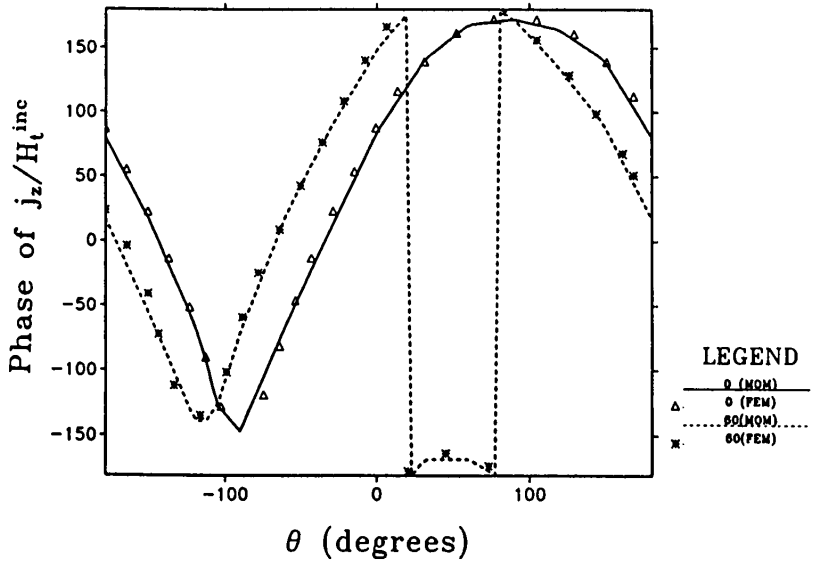

Figure 10.12 Phase of the normalized surface current density as a function of θ for $\phi = 0°$ and $\phi^i = 60°$. Parameters are $a = 0.125$, $\epsilon_r = 4$, $h = -0.065$ (TM_z case).

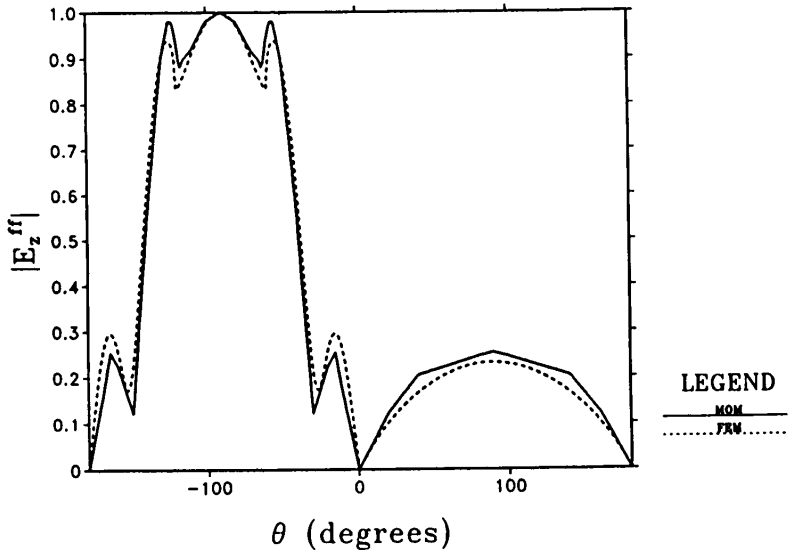

Figure 10.13 Plot of $|E_z^{ff}|$ as a function of θ for $a = 0.175, \phi^i = 0, \epsilon_r = 4$, $h = -0.175, \epsilon_{rd} = 8$ (TM_z case).

In order to obtain accurate results for this size cylinder, 8000 elements are used to mesh the cylinder. The field pattern $|E_z^{ff}(\theta)|$ is shown in Fig. 10.14. To demonstrate the capabilities of the bymoment method in handling arbitrary shapes and inhomogeneities, we consider the case of two dielectric cylinders. Each cylinder has a radius of $a = 0.3$, and their centers are separated by a distance of one free space wavelength. The mesh used for such a case is shown in Fig. 10.15. The boundaries of cylinders are located two elements inside the mesh on the left and right side of the geometry. For the first case, the cylinders are located in the upper half-space with $h = 0.35$, $\epsilon_{rd} = 4$, and $\phi^i = 0°$. Curves are shown in Fig. 10.16 for the field pattern when $\epsilon_r = 1$ and $\epsilon_r = 4$. The free space result ($\epsilon_r = 1$) agrees with the result shown in [2]. It is interesting to note that the forward scatter is focussed by the presence of the interface and the backscatter is suppressed. Let us next consider the case where the two cylinders are buried in the lower half-space. We choose $h = -0.35$, $\epsilon_{rd} = 8$, $\epsilon_r = 4$, and $\phi^i = 0°$. The result is shown in Fig. 10.17.

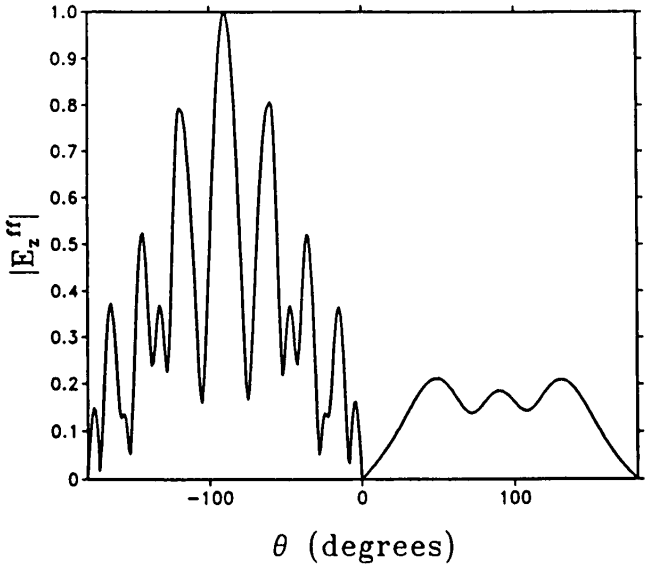

Figure 10.14 Plot of $|E_z^{ff}|$ as a function of θ for $a = 0.6$, $\phi^i = 0$, $\epsilon_r = 4$, $h = -0.65$, $\epsilon_{rd} = 8$ (TM_z case).

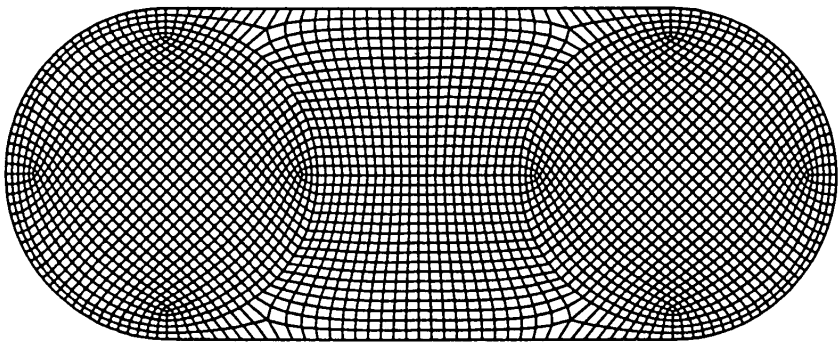

Figure 10.15 FEM mesh for the two dielectric cylinders case.

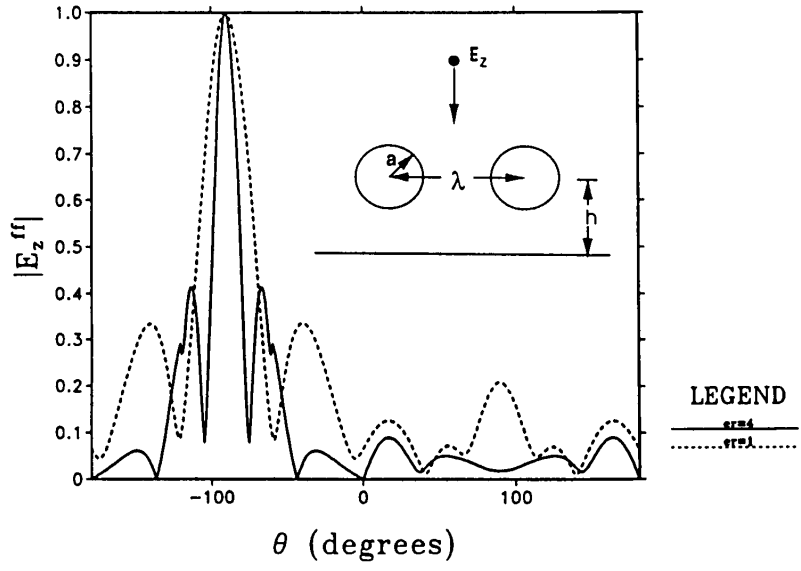

Figure 10.16 Plot of $|E_z^{ff}|$ as a function of θ for two dielectric cylinders with $a = 0.3$, $\phi^i = 0$, $h = 0.35$, $\epsilon_{rd} = 4$ (TM_z case).

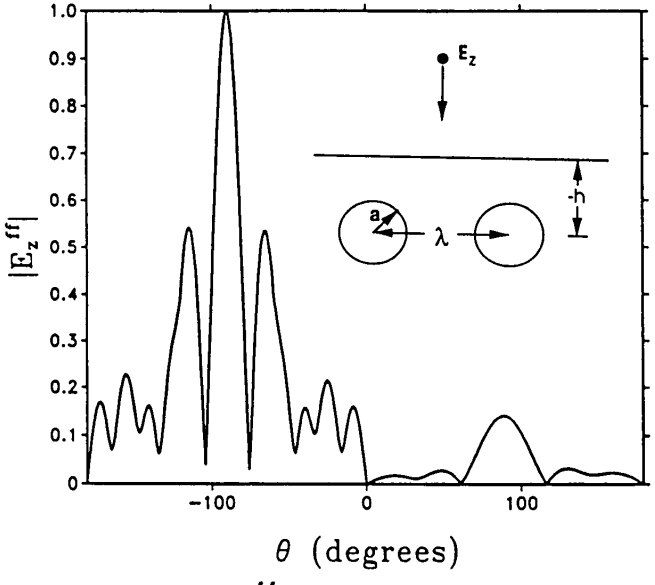

Figure 10.17 Plot of $|E_z^{ff}|$ as a function of θ for two dielectric cylinders with $a = 0.3$, $\phi^i = 0$, $\epsilon_r = 4$, $h = -0.35$, $\epsilon_{rd} = 8$ (TM_z case).

10.5 Summary

In this chapter, we formulate and solve the problem of scattering from a cylinder in the presence of an interface using the bymoment method. The cylinder's cross-section and material properties are assumed to be arbitrary. The placement of the cylinder with respect to the interface may also be arbitrary. The formulation is given in terms of the TE_z polarization although this formulation can easily be modified for the TM_z case.

We begin by considering the solution interior to the cylinder. The interior solution can be generated by using the finite-element method if the solution on the boundary of the finite-element mesh is known. The solution is not known, but we can represent the solution on the boundary of the mesh in terms of a sum of unknown coefficients, each of which is multiplied by known functions Ψ_n. These known functions form a complete set of basis functions on the boundary of the mesh. We can therefore solve a set of finite-element problems using the Ψ_n's as boundary conditions to obtain a set of finite-element solutions. By summing up these solutions with the appropriate coefficients, we obtain the correct solution inside the cylinder. Thus, the problem is reduced to one of finding these coefficients. In order to do this, we apply Green's theorem to the region exterior to the cylinder using a set of linearly independent testing functions which satisfy the Helmholtz equation, the Sommerfeld radiation condition, and the boundary conditions at the interface. For our case, we choose the Green's function for our geometry without the cylinder. The placement of the sources for the Green's function cannot be arbitrary. In this paper, we provide reasons for this. Also, a guideline is given for the placement of the sources.

We validate our method by writing a computer program to compare our results to that given in the literature. Because of the interface, the numerical evaluation of the testing function is rather intensive. Therefore, the majority of the computation time is spent on the evaluation of the testing functions. Results are provided for both the perfectly conducting circular cylinder and the dielectric circular cylinder. The agreement between the method of moment and bymoment results validates our method.

References

[1] Cangellaris, A. C., and R. Lee, "The bymoment method for two-dimensional electromagnetic scattering," submitted to *IEEE Trans. Antennas Propagat.,* May 1989.

[2] Lee, R., and A. C. Cangellaris, "Electromagnetic scattering from multiple cylinders using the bymoment method," submitted to *Radio Science,* Sept. 1989.

[3] Chang, S. K., "Multipole expansion technique for electromagnetic scattering by buried objects," *Electromagnetics,* **1**, 73–89, 1981.

[4] Hohmann, G. W., "Electromagnetic scattering by conductors in the earth near a line source of current," *Geophysics,* **36**, 101–131, 1971.

[5] Parry, J. R., and S. H. Ward, "Electromagnetic scattering from cylinders of arbitrary cross-section in a conductive half-space," *Geophysics*, **36**, 67–100, 1971.

[6] Howard, A. Q., "The electromagnetic fields of a subterranean cylindrical inhomogeneity excited by a line source," *Geophysics,* **37**, 975–984, 1972.

[7] Mahmoud, S. F., S. M. Ali, and J. R. Wait, "Electromagnetic scattering from a buried cylindrical inhomogeneity inside a lossy earth," *Radio Science,* **16**, 1285–1298, 1981.

[8] Howard, A. Q., and J. L. Kretzschmar, "Synthesis of EM geophysical tomographic data," *Proc. IEEE,* **74**, 353–360, 1986.

[9] Butler, C. M., X. Xu, and A. W. Glisson, "Current induced on a conducting cylinder located near the planar interface between two semi-infinite half-spaces," *IEEE Trans. Antennas Propagat.,* **AP–33**, 616–624, 1985.

[10] Xu, X., and C. M. Butler, "Current induced by TE excitation on a conducting cylinder located near the planar interface between two semi-infinite half-spaces," *IEEE Trans. Antennas Propagat.,* **AP–34**, 880–890, 1986.

[11] Xu, X., and C. M. Butler, "Scattering of TM excitation by coupled and partially buried cylinders at the interface between two media," *IEEE Trans. Antennas Propagat.,* **AP–35**, 529–538, 1987.

[12] Becker, E. B., G. F. Carey, and J. T. Oden, *Finite Elements: An Introduction*, Prentice-Hall, Inc., Englewood Cliffs, New Jersey, 1981.

[13] Harrington, R. F., *Time-Harmonic Electromagnetic Fields*, McGraw-Hill, New York, 1961.

[14] Felsen, L. B., and N. Marcuvitz, *Radiation and Scattering of Waves*, Prentice-Hall, Inc., Englewood Cliffs, New Jersey, 1951.

[15] Baertlein, B. A., *Frequency Response of E-Polarized Sources over a Lossy Earth in the Presence of Two-Dimensional Shielding Structures*, Ph.D. Dissertation, ECE Dept., University of Arizona, Tucson, Arizona 85721, 1988.

[16] Johnson, W. A., and D. G. Dudley, "Real axis integration of sommerfeld integrals: source and observation points in air," *Radio Science*, **18**, 175–186, 1983.

[17] Blacker, T. D., "FASTQ User Manual, Version 1.2," Sandia Report, SAND88-1326, July 1988.

[18] Wait, J. R., *Electromagnetic Wave Theory*, Harper and Row, New York, 1985.

[19] Butler, C. M., private communication, Sept. 1989.